*Limnol. Oceanogr.*, 46(3), 2001, 632–643


# Spatial and diurnal dynamics of dissolved organic matter (DOM) fluorescence and $H_2O_2$ and the photochemical oxygen demand of surface water DOM across the subtropical Atlantic Ocean

*Ingrid Obernosterer, Piet Ruardij, and Gerhard J. Herndl*[1]
Department of Biological Oceanography, Netherlands Institute for Sea Research (NIOZ), P.O. Box 59, 1790 AB Den Burg, Texel, The Netherlands

*Abstract*

Diurnal dynamics of dissolved organic matter (DOM) fluorescence and hydrogen peroxide ($H_2O_2$) concentrations were followed in the upper 100 m of the water column at five stations across the subtropical Atlantic Ocean in July and August 1996. The 10% levels of surface solar radiation for the ultraviolet (UV) B range (at 305- and 320-nm wavelengths) were at 16 and 23 m in depth and for the UVA range (at 340- and 380-nm wavelengths) were at 35 and 63 m in depth, respectively. The DOM fluorescence decreased over the course of the day, whereas $H_2O_2$ concentrations increased, especially in the diurnally stratified surface water layers extending to 10–50-m depth. In situ $H_2O_2$ net production varied between 5.5 nmol $L^{-1}$ $h^{-1}$ at 5-m depth and 1 nmol $L^{-1}$ $h^{-1}$ at 40-m depth, resulting in an $H_2O_2$ net production of ~38 $\mu$mol $m^{-2}$ $d^{-1}$ in the upper 50 m of the water column. Photochemical oxygen ($O_2$) demand of water collected at 10-m depth in the early morning and exposed to surface solar radiation varied between 0.9 and 2.8 $\mu$mol $O_2$ $L^{-1}$ $d^{-1}$ and was found to be consistently higher (by a 1.3–8.3-fold measure) than bacterial respiration (measured in 0.8 $\mu$m–filtered seawater in the dark). UVB radiation was responsible for 0–30% of the photochemical $O_2$ demand. A simple one-dimensional physical model was combined with a photochemical/biological model in order to describe the photochemical production of $H_2O_2$ at different depth layers over the course of the day and to determine the contribution of physical versus biological processes in terms of the loss of $H_2O_2$ from the surface layers in the late afternoon. The model reflects well the observed diurnal $H_2O_2$ dynamics. It further provides evidence that mainly biological breakdown determines the loss of $H_2O_2$ in the upper 50 m of the water column during the day; however, in the late afternoon, vertical mixing is important in transporting $H_2O_2$ from the uppermost 5-m layer to the 10–20-m layers.

Stratospheric ozone depletion has caused an increase in ground-level ultraviolet (UV) B radiation (280–320 nm), particularly in polar regions (Crutzen 1992) but also in temperate latitudes (Stolarski et al. 1992). In the subtropical zone, UVB radiation is stable, although it is much greater (≈10-fold) than that observed in Antarctica, even when the atmosphere over Antarctica is depleted in ozone (Holm-Hansen et al. 1993). UVB radiation accounts for only <1% of the total radiation intensity reaching the Earth's surface; nevertheless, it is a highly reactive component of sunlight. Direct exposure to UV radiation has been shown to be detrimental to aquatic organisms (Smith 1989; Cullen et al. 1992; Herndl et al. 1993). UV radiation, however, can also indirectly affect biological processes via photochemical alteration of dissolved organic matter (DOM), which might either stimulate (*see* review by Moran and Zepp 1997) or inhibit microbial activity (Benner and Biddanda 1998; Tranvik and Kokalj 1998; Obernosterer et al. 1999).

The absorption of solar radiation (particularly in the UV range) by chromophoric DOM can lead to a variety of photochemical reactions. The organic chromophores can react either directly or indirectly as photosensitizers in reactions with other substrates (Zafiriou et al. 1984; Cooper and Lean 1989). Along with an overall loss in absorbance and fluorescence (Vodacek 1992; Morris and Hargreaves 1997), changes in the chemical and biological reactivity of the DOM have been reported (Zafiriou et al. 1984; Moran and Zepp 1997). Photochemical transformations of DOM have been shown to result in the formation of inorganic carbon (DIC) species, such as CO and $CO_2$ (Mopper et al. 1991; Miller and Zepp 1995; Graneli et al. 1996), a variety of low–molecular weight organic compounds—such as carbonyl compounds (Kieber et al. 1989; Bertilsson and Tranvik 1998) and amino acids (Amador et al. 1989), and inorganic nitrogen (Bushaw et al. 1996) and phosphorous (Francko and Heath 1982). However, only a small fraction of the photoproducts formed from DOM has been identified thus far (Moran and Zepp 1997).

The interaction of UV radiation with DOM can also result in the formation of reactive oxygen species. Hydrogen peroxide ($H_2O_2$) is the least reactive of the reduced oxygen species and is formed in sunlight-initiated redox reactions involving DOM, $O_2$, and trace metals (Cooper and Zika 1983; Zika et al. 1985). Its stability, relative to other photochemically produced reduced-oxygen species, makes it a useful tracer for DOM photolysis. Photochemical formation

[1] Corresponding author.

*Acknowledgments*

We thank the captain and the crew of the Dutch Royal Navy on Hr.Ms. *Tydeman* for the excellent cooperation and assistance with the radiation measurements. S. Gonzalez performed the DOC analysis. The cruise was supported by the Netherlands Geoscience Foundation of the Netherlands Organization for Scientific Research. Additional funding was provided by NIOZ and the CEC Environment and Climate Program (EV5V-CT 94-0512). This work is in partial fulfillment of the requirements for a Ph.D. degree from the University of Groningen by I.O. This is publication 3495 of the NIOZ.

is considered to be the major production mechanism of $H_2O_2$ in surface waters. However, biological (Palenik et al. 1987; Roncel et al. 1989) and chemical (Moffet and Zika 1983) formation of $H_2O_2$ as well as wet and dry deposition (Weller and Schrems 1993; Miller and Kester 1994) can also contribute to the $H_2O_2$ concentration in the upper water column. Several studies indicate that microbial processes play an important role in the decomposition of $H_2O_2$ (Cooper and Lean 1989); however, little is known with regard to the relative importance of chemical processes in the decomposition of $H_2O_2$.

$H_2O_2$ has also been used as a sensitive tracer for diurnal stratification (Sikorski and Zika 1993; Scully and Vincent 1997). Diurnal thermoclines are known to occur in the upper ocean when solar heating causes a temperature increase in the surface layers (Imberger 1985; Price et al. 1986). Depending on the intensity of solar radiation, wind stress, and optical properties of the water column, this diurnal stratification can extend down to a 40-m depth (Price et al. 1986), thereby entrapping DOM and planktonic organisms in the sunlit surface layer over almost an entire diurnal cycle. The extension and the stability of the diurnal thermocline should therefore determine irradiation-related processes in this layer.

The objectives of this study were to evaluate the spatial and diurnal dynamics of DOM fluorescence and $H_2O_2$ concentrations in the upper 100 m of the water column across the subtropical Atlantic Ocean. These photoinduced processes were resolved, with special emphasis on the surface layers subjected to diurnal stratification. We also developed a simple model in order to describe the photochemical production of $H_2O_2$ and to evaluate the importance of biological versus physical processes for the dynamics of $H_2O_2$ in the top 50-m layers. Furthermore, the photochemical oxygen ($O_2$) demand was measured and related to bacterial respiration. To our knowledge, this is the first report on the photochemical $O_2$ demand of the surface layers of the oligotrophic subtropical ocean.

## Materials and methods

*Study sites*—The study was carried out during a cruise in the subtropical Atlantic on the RV Hr.Ms. *Tydeman.* Five stations (Sta. I, 12°N, 48°W; Sta. II, 14°N, 40°W; Sta. III, 23°N, 38°W; Sta. IV, 34°N, 35°W; and Sta. V, 34°N, 23°W), each occupied for 4 d, were sampled during July and August 1996. Based on the comparatively low salinity (~36.05) of the top 50 m of the water column of Sta. I, we consider this station to be influenced by freshwater originating from the South American continent, whereas Sta. II–V (mean salinity, 36.93; range, 36.50–37.60) are considered truly oceanic. A pronounced deep chlorophyll maximum was detectable at all stations at 80–130-m depth.

*Irradiance measurements*—Surface and underwater irradiance were measured at 305-, 320-, 340-, and 380-nm wavelengths and in the photosynthetic active radiation (PAR; 400–700-nm) range with a Biospherical PUV-500 radiometer using the correction factor for the 305-nm channel, as suggested by Kirk (1994). Surface irradiance measurements and irradiance-depth profiles were carried out over a 2–4-d period per station, with more frequent measurements (every 2–4 h) over 1–2 d. Integrated daily surface irradiance was calculated from the surface irradiance recorded at the upper deck of the ship every 2–4 h. Additionally, at Sta. I and V, surface irradiance was recorded at 10-min intervals and was integrated over the time period between 0800 and 1900 h. Diffuse attenuation coefficients for downward irradiance (Kd) were determined from the slope of the linear regression of the log-transformed downwelling irradiance versus depth. For calculating Kd, irradiance measurements were taken from the upper 30 m of the water column only. Below this depth layer, no linear relationship was obtained between the log-transformed irradiance and depth, probably because of the increasing absorbance by plant pigments toward the deep chlorophyll maximum layers. The number of individual irradiance measurements used to determine Kd was >100 per profile, and correlation coefficients were always >0.97.

*Temperature profiles*—Measurements of temperature profiles were performed concurrently with the irradiance measurements with the PUV-500 radiometer, set at a recording interval of 1 s. The accuracy of the temperature sensor of this instrument is 0.03°C (Biospherical pers. comm.).

*Depth profiles of hydrogen peroxide ($H_2O_2$) and DOM fluorescence*—At each station, series of CTD hydrocasts (SeaBird) were performed over diel cycles down to 200 m depth at 2–4-h intervals. Water samples for the determination of $H_2O_2$ concentrations and DOM fluorescence were taken with 10-liter NOEX bottles mounted on the CTD frame. Additionally, at Sta. IV and V, surface water (top 50 cm) was sampled using an acid-rinsed polyvinyl chloride bucket. At each station, diel variations in $H_2O_2$ concentration and DOM fluorescence were followed in the upper-100-m water column over two consecutive days. In situ $H_2O_2$ net production rates were calculated from the increase in $H_2O_2$ concentration at a specific depth over daytime (from 0800 to 1500 h) using linear regression analysis. Only data sets with at least three $H_2O_2$ concentrations over this time period and exhibiting a $r^2 > 0.7$ were used for calculating in situ $H_2O_2$ net production rates.

*Photochemical production of $H_2O_2$ in 0.2-$\mu$m–filtered seawater*—At Sta. I, a 2-liter water sample was taken at 5-m depth shortly before dawn and immediately filtered through 0.2-$\mu$m polycarbonate filters (Nuclepore; 47-mm filter diameter, rinsed with Milli-Q water and surface seawater prior to filtration). The 0.2-$\mu$m filtrate was subsequently transferred to 120-ml quartz biological oxygen demand (BOD) bottles and exposed to surface solar radiation levels of between 1030 and 1600 h. Exposure to surface solar radiation was performed in triplicate, with one dark control wrapped in aluminum foil and incubated in a water bath connected to a running seawater system. All the solar irradiation–exposed BOD bottles and the dark control were subsampled (20 ml) after 1, 2.5, 4, and 7.5 h for the determination of $H_2O_2$ concentrations (described below). $H_2O_2$ concentrations in the dark treatments increased by 32 nM after 1.5 h and were stable thereafter; irradiation-exposed treatments were subsequently corrected for this increase in $H_2O_2$ concentration in the dark controls. $H_2O_2$ gross production rates were determined from the linear increase of $H_2O_2$ over time.

*Photochemical oxygen demand of DOM and bacterial respiration*—At Sta. II–V, water was collected at 10-m depth shortly before dawn and immediately filtered through either 0.8- or 0.2-$\mu$m polycarbonate filters (Nuclepore; 47-mm filter diameter) after rinsing the filters as described above. To determine the photochemical $O_2$ demand of the surface water DOM, the 0.2-$\mu$m filtrate was transferred to quartz BOD bottles (~120 ml) and exposed to surface solar radiation for 1–2 d. In order to determine the contribution of the UVB wavelength range on the photochemical $O_2$ demand, one set of samples was exposed to the full range of surface-level solar radiation and one set was wrapped in Mylar-D foil to shield off the UVB range. Dark controls were wrapped in aluminum foil. To compare the photochemical $O_2$ demand with bacterial respiration, 0.8-$\mu$m–filtered water was incubated in BOD bottles (~120 ml) in the dark. For both, photochemical and bacterial $O_2$ consumption, all the incubations (including the dark controls) were performed in triplicate in a water bath connected to a running seawater system to maintain in situ temperature conditions of the surface layers (~25°C). The initial dissolved $O_2$ concentration was measured also in triplicate. Photochemical $O_2$ demand was calculated from the difference in the dissolved $O_2$ concentration in the 0.2-$\mu$m filtrate between the irradiation-exposed and the dark treatments at the end of the 1–2-d incubation period. Bacterial respiration was calculated from the difference in the dissolved $O_2$ concentration in the 0.8-$\mu$m filtrate at the beginning and the end of the incubation period (1–2 d).

*Hydrogen peroxide ($H_2O_2$) determination*—$H_2O_2$ concentrations were measured using the enzyme-catalyzed dimerization of *P* hydroxyphenylacetic acid (POHPAA) into a fluorescent product (Miller and Kester 1988). All chemicals were obtained from Sigma Chemicals. The peroxidase stock solution was prepared in the laboratory and was kept frozen in 2-ml Eppendorf vials. The POHPAA stock solution (25 mM, prepared in Milli-Q water) was kept refrigerated during the 4 d of sampling per station. The POHPAA working solution was prepared daily in 0.25 M Tris buffer. Peroxidase (10,440 U $L^{-1}$) and POHPAA (255 $\mu$M) working solutions were mixed (1 : 1) resulting in a fluorogenic reagent that was subsequently added to the water samples. $H_2O_2$ standards were also freshly prepared daily by serially diluting the $H_2O_2$ stock solution (1 mM) with Milli-Q water.

All samples were immediately derivatized by adding the fluorogenic reagent (peroxidase and POHPAA) to a 5-ml sample. Samples were incubated in triplicate at in situ temperature (~25°C) in the dark for 30 min before the fluorescence was measured with a Jasco 820 spectrofluorometer. $H_2O_2$ concentrations in the samples were calculated using the daily established slope for standard additions (5–200 nM). Blanks were determined by adding the fluorogenic reagent to samples treated with catalase for 5 min (Miller and Kester 1988). The detection limit defined as three times the standard deviation of the blank was, on average, 4.0 ± 1.8 nM ($n$ = 10) for the five stations.

*Determination of dissolved oxygen*—The concentration of dissolved $O_2$ was measured via the spectrophotometric determination of total iodine (Pai et al. 1993; Roland et al. 1999). Sample treatment principally followed the standard protocol for the determination of $O_2$ by Winkler titration (Parsons et al. 1984). The amount of iodine was measured spectrophotometrically at a wavelength of 456 nm using a Hitachi U-1000 spectrophotometer and a 1-cm flow-through cuvette. The sample was withdrawn from the BOD bottle with a sipper system; the end of the inlet tube was placed near the bottom of the BOD bottle in order to avoid possible loss of volatile iodine. The instrument was zeroed against Milli-Q water. Calibration was performed by standard additions of iodate to distilled water, resulting in an empirical coefficient of 0.54455 nM $cm^{-1}$ for the 456-nm wavelength (Kraay pers. comm.). A four-digit voltmeter (Metex M4650) was connected to the spectrophotometer in order to increase the sensitivity of the absorption readings. All incubations were done in triplicate; the analytical standard deviation was <0.5% ($n$ = 42).

*Dissolved organic carbon (DOC) analysis*—Samples for DOC were filtered through presoaked and rinsed (with distilled water) 0.2-$\mu$m polycarbonate filters (Nuclepore) using combusted (450°C for 4 h) glass filtration sets. Duplicate 8-ml subsamples from the 0.2-$\mu$m filtrate were subsequently acidified with three drops of concentrated phosphoric acid (45% w/v) and sealed in combusted 10-ml ampoules. Samples were stored at 4°C for later analysis. DOC was measured by injecting 50 $\mu$l of sample into a Shimadzu TOC-5000A (Benner and Strom 1993). The DOC content was determined after sparging the samples with $CO_2$-free air. Standards were prepared with potassium hydrogen biphthalate (Kanto Chemical Co). The blank was, on average, ~15.2 ± 7.7 $\mu$M C (range 5–32 $\mu$M C), and the average analytical precision of the instrument was <4%.

*DOM fluorescence measurements*—The fluorescence of the DOM was measured on raw seawater immediately after collection from the NEOX bottles at an excitation wavelength of 350 nm and an emission wavelength of 450 nm using a 1-cm quartz cuvette. The fluorometer (Jasco 820) was standardized with a quinine sulfate solution (1 QSU = 1 ppb quinine sulfate in 0.05 M $H_2SO_4$).

*Statistical analysis*—A one-way analysis of variance (ANOVA) with a multiple post hoc (Tukey) test was used to check for differences among the five stations. The Wilcoxon test was used to check for treatment effects (full solar radiation versus exclusion of UVB) on variables. Statistics were performed with SYSTAT 5.2 (Wilkinson 1990).

*Description of the model*—A one-dimensional physical model based on the Princeton Ocean Model (Blumberg and Mellor 1987) was combined with a simple photochemical/biological model (*see* for details the Web Appendix at http://www.aslo.org/lo/pdf/vol_46/issue_3/0632a1.pdf) in order to describe the diurnal changes in $H_2O_2$ concentrations and to evaluate the importance of physical versus biological processes on the dynamics of $H_2O_2$ at different depth layers of

Table 1. Diel-integrated irradiance above the sea surface and at 5-m depth for the UVB (at 305- and 320-nm wavelengths) and the UVA (at 340- and 380-nm wavelengths) regions (in kJ $m^{-2}$ $nm^{-1}$ $d^{-1}$) and for photosynthetic active radiation (PAR) (400–700 nm, in E $m^{-2}$ $d^{-1}$) at Sta. I–V. All the measurements were performed on nearly cloudless days.

| Sta. | UVB (kJ $m^{-2}$ $nm^{-1}$ $d^{-1}$) | | UVA (kJ $m^{-2}$ $nm^{-1}$ $d^{-1}$) | | PAR (E $m^{-2}$ $d^{-1}$) |
|---|---|---|---|---|---|
| Surface | 305 nm | 320 nm | 340 nm | 380 nm | |
| I | 1.7 | 7.6 | 14.0 | 19.3 | 52 |
| II | 1.6 | 7.0 | 12.7 | 17.4 | 46 |
| III | 1.4 | 7.0 | 13.2 | 18.5 | 51 |
| IV | 1.0 | 5.9 | 11.8 | 16.7 | 46 |
| V | 0.9 | 5.5 | 11.0 | 15.6 | 45 |
| 5-m Depth | | | | | |
| I | 0.3 | 2.9 | 7.4 | 13.0 | 24 |
| II | 0.8 | 5.1 | 10.1 | 16.9 | 34 |
| III | 0.7 | 4.5 | 10.2 | 16.9 | 31 |
| IV | 0.4 | 4.0 | 9.1 | 16.6 | 26 |
| V | 0.3 | 3.2 | 6.5 | 12.1 | 24 |

the upper–50-m water column. For the model we assume that the processes regulating diurnal $H_2O_2$ dynamics are the same at all five stations. The physical model describes the diel hydrodynamics, including the development of a diurnal thermocline as forced by air temperature, humidity, cloud cover, wind speed, and irradiance. These parameters were measured during the cruise on board the ship. The photochemical production of $H_2O_2$ in the upper–50-m water column is modeled using measured surface solar irradiance, the Kd, and the DOC concentration (Cooper et al. 1994). In our model, diurnal $H_2O_2$ dynamics in different depth layers are determined by the photochemical production of $H_2O_2$, its decomposition by bacterioplankton (Cooper and Lean 1992; Cooper et al. 1994), and vertical mixing (included in the physical model). The biological decomposition of $H_2O_2$ is regulated enzymatically (Moffet and Zafiriou 1990), and in the model it is dependent on the concentration of $H_2O_2$ and the enzymes. The enzyme production is related to both the bacterioplankton activity and the increase in $H_2O_2$ concentration over time. Modeled bacterioplankton activity is, on the one hand, related to primary production, which is estimated from measured PAR intensities. On the other hand, high levels of UV radiation inhibit bacterioplankton activity in the present model (Herndl et al. 1993); this inhibitory period is followed by a rapid recovery due to decreasing irradiation intensities in the late afternoon and a decline in the ratio of UVB to UVA radiation (Kaiser and Herndl 1997).

## Results

*Surface solar radiation and irradiance-depth profiles*—Surface solar radiation during cloudless days integrated over the photoperiod ranged between 0.9 and 1.7 kJ $m^{-2}$ $nm^{-1}$ $d^{-1}$ (for 305 nm), between 5.5 and 7.6 kJ $m^{-2}$ $nm^{-1}$ $d^{-1}$ (for 320 nm), between 11 and 14 kJ $m^{-2}$ $nm^{-1}$ $d^{-1}$ (for 340 nm), and between 15.6 and 19.3 kJ $m^{-2}$ $nm^{-1}$ $d^{-1}$ (for 380 nm) at the five stations (Table 1). PAR varied between 45 and 52 E $m^{-2}$ $d^{-1}$.

At the five stations, mean attenuation coefficients (Kd) varied in the UVB region between 0.126 and 0.156 $m^{-1}$ (for 305 nm) and between 0.088 and 0.105 $m^{-1}$ (for 320 nm) (Table 2). Thus, the 10% surface radiation levels for the 305- and 320-nm wavelengths were at 16 $\pm$ 1.5 and 23 $\pm$ 1.8 m in depth, respectively (Table 2). Mean Kd for the UVA wavelength range varied between 0.056 and 0.069 $m^{-1}$ (for 340 nm) and between 0.031 and 0.041 $m^{-1}$ (for 380 nm), resulting in mean 10% surface radiation levels at 35 $\pm$ 3.4 and 63 $\pm$ 7.5 m in depth, respectively (Table 2). The Kd for PAR were similar to those for 380 nm (Table 2). Among the five stations, Sta. III exhibited the lowest Kd for all wavelengths; however, only $Kd_{305\ nm}$ was found to be significantly lower at Sta. III than at Sta. I, IV, and V (ANOVA, $P$ = 0.014). The highest Kd for 305 and 320 nm were generally detected in the morning and decreased at all stations (by about 7%) until 1300 h. From 1300–1700 h, a further decrease in the $Kd_{305\ nm}$ was detectable at two out of four stations, whereas at the other two stations, the $Kd_{305\ nm}$ was higher at 1700 h than at 1300 h. The $Kd_{320\ nm}$ increased at all stations in the late afternoon (Table 3).

*DOC and DOM fluorescence—Spatial aspects*—DOC concentrations generally declined from the surface mixed layer to 150 m in depth. Mean DOC concentrations in surface waters ranged between 76.5 and 90.6 $\mu$M C; at 150 m in depth, DOC concentrations varied between 57.4 and 70.5 $\mu$M (Table 4). Fluorescence, expressed as DOC-normalized quinine sulfate units, was two to six times lower at the 50-m depth than at the 150-m depth (Table 4). At Sta. II and III, DOM fluorescence at the 50-m depth was significantly lower than at Sta. I, IV, and V (ANOVA, $P < 0.001$).

Table 2. Mean attenuation coefficients (Kd $m^{-1}$) of the UVB (at 305- and 320-nm wavelengths) and UVA (at 340- and 380-nm wavelengths) ranges and of photosynthetic active radiation (PAR) (400–700 nm) at Sta. I–V. Kd were calculated from measurements performed around noon on consecutive days; $n$ = number of depth profiles from which Kd were calculated ($\pm$SD).

| Sta. | $n$ | $Kd_{305\ nm}$ | $Kd_{320\ nm}$ | $Kd_{340\ nm}$ | $Kd_{380\ nm}$ | $Kd_{PAR}$ |
|---|---|---|---|---|---|---|
| I | 3 | 1.155 (0.006) | 0.105 (0.004) | 0.068 (0.005) | 0.041 (0.003) | 0.038 (0.002) |
| II | 4 | 0.140 (0.011) | 0.104 (0.009) | 0.069 (0.007) | 0.041 (0.012) | 0.038 (0.014) |
| III | 2 | 0.126 (0.004) | 0.088 (0.004) | 0.056 (0.004) | 0.031 (0.001) | 0.034 (0.001) |
| IV | 4 | 0.151 (0.008) | 0.103 (0.008) | 0.069 (0.007) | 0.035 (0.009) | 0.041 (0.005) |
| V | 3 | 0.156 (0.006) | 0.105 (0.003) | 0.069 (0.006) | 0.036 (0.004) | 0.050 (0.001) |

Table 3. Diurnal variation of the attenuation coefficients (Kd $m^{-1}$) at 305- and 320-nm wavelengths at Sta. I–V. At Sta. IV and V, Kd are mean values of measurements taken on two consecutive days; SD was always <5%; nd, not determined.

| | Time of day | Sta. I | II | III | IV | V |
|---|---|---|---|---|---|---|
| $Kd_{305\ nm}$ | 0900 | 0.171 | 0.143 | 0.133 | 0.150 | 0.174 |
| | 1300 | 0.162 | 0.135 | 0.123 | 0.146 | 0.155 |
| | 1530 | nd | nd | nd | 0.138 | 0.150 |
| | 1700 | 0.128 | nd | 0.138 | 0.110 | 0.166 |
| $Kd_{320\ nm}$ | 0900 | 0.116 | 0.103 | 0.095 | 0.107 | 0.109 |
| | 1300 | 0.110 | 0.102 | 0.085 | 0.100 | 0.103 |
| | 1530 | nd | nd | nd | 0.106 | 0.108 |
| | 1700 | 0.112 | 0.112 | 0.099 | 0.106 | 0.105 |

*Stratification and dynamics of DOM fluorescence and $H_2O_2$—Diurnal aspects*—Temperature, DOM fluorescence, and $H_2O_2$ concentrations were followed in the upper 100 m of the water column over diurnal cycles (Fig. 1). To determine whether the same water mass has been sampled throughout the day, we compared the measured and modeled salinity depth profiles at the corresponding sampling times. Pronounced differences between the measured salinity and the salinity derived from the one-dimensional physical model (>0.06 psu) were detectable at Sta. I (from 0 to 50 m in depth) and IV (>20 m in depth) between ~1100 h and 1500 h. This could indicate the temporary presence of a different water mass as a result of lateral transport. Thus, the observed changes in DOM fluorescence and $H_2O_2$ concentration at Sta. I and IV are most likely influenced by changing hydrographic conditions.

Temperature profiles indicate a pronounced diurnal stratification in the upper 10 to 50 m of the water column at all stations (Fig. 1). At Sta. IV and V, a shallow permanent thermocline was detectable at around 30 m in depth, and a diurnal stratification reached to ≈15 m in depth (Fig. 1). The diurnal increase in surface water (0–50-m layer) temperature varied between 0.35 and 1.5°C, with the highest temperatures reached in the early afternoon. This warming of the uppermost water layers during the day at all stations was followed by mixing events in the late afternoon (as a result of surface cooling). This trend was particularly pronounced at Sta. II and III, as reflected by the temperature profiles taken at 1700 h (Fig. 1).

DOM fluorescence (given in DOC-normalized QSU) decreased during the day at all stations. At Sta. II, III, and V, variations in the DOM fluorescence were restricted to the diurnally stratified layers (Fig. 1). The pronounced decrease in DOM fluorescence throughout the upper 50 m of the water column at Sta. I and at Sta. IV at >20 m in depth probably results from changes in the hydrographic conditions, as indicated above.

Although DOM fluorescence decreased during the course of the day, $H_2O_2$ concentrations increased in the uppermost water layers from the morning to the early afternoon (1230–1500 h, Fig. 1). Generally, all $H_2O_2$ concentration profiles revealed a surface maximum (75–220 nM) and a decline with depth. A sharp decline in $H_2O_2$ concentrations was always detectable at the shallow thermocline (30–50 m in depth). At 100 to 150 m in depth, $H_2O_2$ concentrations ranged between 5 and 10 nM (data not shown). Similar to the DOM fluorescence, diurnal dynamics of $H_2O_2$ at Sta. II, III, and V were most pronounced in the upper–20-m water layers, whereas at Sta. I and IV, diurnal variations were detectable down to 50 m in depth (Fig. 1).

We consistently detected a linear increase in $H_2O_2$ concentrations in the individual depth layers (down to 50 m in depth) between 0800 and 1500 h, with highest diurnal in situ net production rates of $H_2O_2$ obtained close to the surface (Table 5). At Sta. II—V, $H_2O_2$ net production rates ranged from 5.5 nmol $L^{-1}$ $h^{-1}$ at 5 m to 1 nmol $L^{-1}$ $h^{-1}$ at 40 m depth (Table 5). At Sta. IV and V, water from the top–50-cm layer was also sampled. In this top–50-cm layer, $H_2O_2$ concentrations did not increase linearly during the course of the day but rather exhibited a sharp peak between 1230 and 1500 h, resulting in in situ net production rate of 42 and 30 nmol $L^{-1}$ $h^{-1}$ at Sta. IV and V, respectively.

*Modeling $H_2O_2$ dynamics*—Modeled $H_2O_2$ dynamics principally followed the same diurnal pattern as the measured

Table 4. Concentration of dissolved organic carbon (DOC, in $\mu$m) and DOM fluorescence normalized to the DOC concentration (in quinine sulfate units [QSU], $\mu$m $DOC^{-1}$) at 50-m and 150-m depths at Sta. 1–V. The mean (±SD) is given for samples taken at different times of the day.

| Depth (m) | Sta. I ($n$ = 3) | II ($n$ = 4) | III ($n$ = 5) | IV ($n$ = 5) | V ($n$ = 5) |
|---|---|---|---|---|---|
| | DOC ($\mu$m) | | | | |
| 50 | 76.5 (2.7) | 90.6 (6.9) | 80.5 (6.8) | 78.2 (5.7) | 81.4 (12.4) |
| 150 | 57.4 (4.4) | 70.5 (8.7) | 64.2 (7.0) | 65.8 (6.2) | 68.6 (15.8) |
| **Depth (m)** | **Sta. I ($n$ = 4)** | **II ($n$ = 7)** | **III ($n$ = 9)** | **IV ($n$ = 8)** | **V ($n$ = 8)** |
| | QSU ($\mu$m DOC) | | | | |
| 50 | 0.0057 (0.0013) | 0.0025 (0.0003) | 0.0022 (0.0002) | 0.0060 (0.0010) | 0.0051 (0.0004) |
| 150 | 0.0157 (0.0013) | 0.0147 (0.0008) | 0.0081 (0.0016) | 0.0104 (0.0008) | 0.0128 (0.0004) |

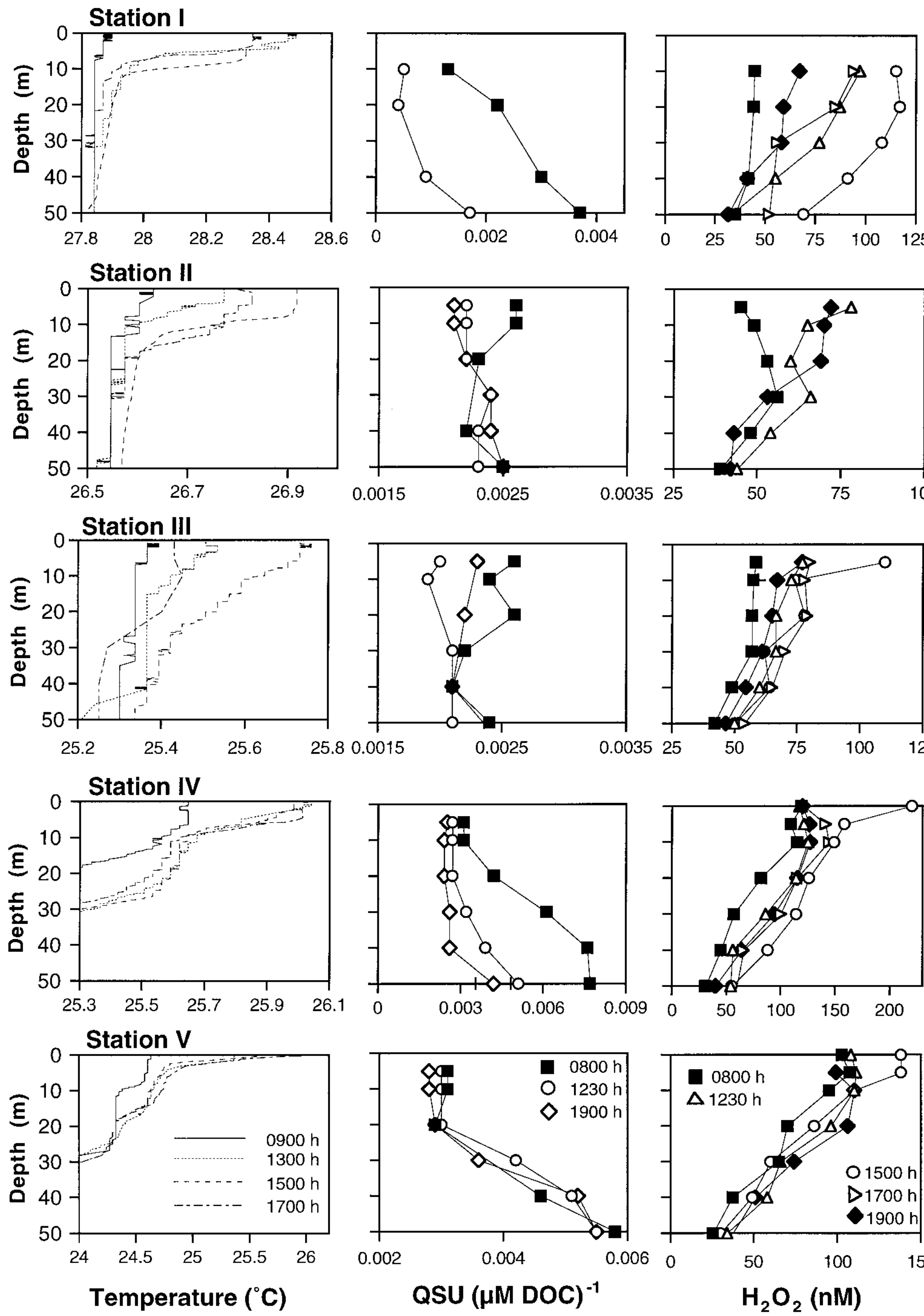


Fig. 1. Diurnal variations in temperature (in °C), DOM fluorescence (in DOC-normalized QSU), and hydrogen peroxide ($H_2O_2$, in nM) in the upper–50-m water column at Sta. I–V; QSU = quinine sulfate units.

$H_2O_2$ concentrations (Fig. 2). The photochemical production of $H_2O_2$ derived from the model led to an increase in $H_2O_2$ concentrations, particularly in the upper 20 m of the water column, during the course of the day. Modeled $H_2O_2$ net production was highest close to the surface around noon, when irradiation intensities are highest and biological decomposition of $H_2O_2$ is probably low due to the generally reduced bacterial activity caused by UV radiation (Herndl et al. 1993). Furthermore, the development of a diurnal thermocline prevents mixing of $H_2O_2$ to deeper water layers. In the late afternoon, the model-derived bacterial activity increased because of a decrease in irradiation intensity. This increased bacterial activity and the concomitant vertical mixing of $H_2O_2$ because the breakup of the diurnal stratification resulted in a decrease in $H_2O_2$ concentrations in the surface layers (Fig. 2). Differences between the observed and the

Table 5. In situ and modeled (in parentheses) net production rates of $H_2O_2$ in different depth layers (nmol $L^{-1}$ $h^{-1}$), which ranged from 5 to 50 m in depth, and daily $H_2O_2$ net production rate ($\mu$mol $m^{-2}$ $d^{-1}$) integrated over the upper 50 m of the water column at Sta. I–V. Daily integrated $H_2O_2$ net production was calculated assuming the same net production rates at 0.1 m as at 5 m in depth and assuming a total exposure period to solar radiation of 7 h; a 7-h period was chosen because of the linear increase in $H_2O_2$ over this time period. No in situ $H_2O_2$ net production rates are given for Sta. 1 and for Sta. IV at >20 m in depth because of the apparently different water masses; nd, not determined.

| Depth | Sta. | | | | |
|---|---|---|---|---|---|
| (m) | I | II | III | IV | V |
| | $H_2O_2$ net production rates (nmol $L^{-1}$ $h^{-1}$) | | | | |
| 5 | nd (8.6) | 5.5 (7.4) | 5.2 (7.5) | 4.8 (4.4) | 3.6 (3.2) |
| 10 | nd (6.3) | 3.6 (6.2) | 2.1 (6.1) | 4.1 (2.3) | 1.8 (1.5) |
| 20 | nd (2.2) | 1.3 (1.9) | 2.5 (3.3) | nd (2.1) | nd (2.1) |
| 30 | nd (0.9) | 1.7 (0.0) | 1.3 (1.2) | nd (0.5) | 0.0 (0.7) |
| 40 | nd (0.5) | 1.0 (0.0) | 1.5 (0.9) | nd (0.3) | 0.0 (0.5) |
| 50 | nd (0.4) | 0.0 (1.0) | 0.0 (0.6) | nd (0.3) | 0.0 (0.0) |
| | Integrated $H_2O_2$ net production rates ($\mu$mol $m^{-2}$ $d^{-1}$) | | | | |
| 0.1–50 | nd (52) | 38 (44) | 38 (56) | nd (28) | nd (26) |

modeled $H_2O_2$ concentrations were highest for Sta. I and for Sta. IV at >20 m in depth, where different water masses were encountered during the course of the observations, as revealed by salinity profiles.

*Photochemical $H_2O_2$ production and $O_2$ demand*—At Sta. I, 0.2-$\mu$m–filtered water from the 5-m depth was exposed to surface solar radiation, and the increase in $H_2O_2$ concentration followed over time. A linear increase in $H_2O_2$ concentration was observed over the incubation period (1030–1600 h, $r^2 = 0.984$), resulting in a $H_2O_2$ gross production rate of 39.8 ± 12.5 nmol $L^{-1}$ $h^{-1}$ ($n = 3$, data not shown).

Photochemical $O_2$ demand of water sampled at the 10-m depth at Sta. II—V and exposed to the full range of surface solar radiation varied between 0.9 and 2.8 $\mu$mol $O_2$ $L^{-1}$ $d^{-1}$ (Fig. 3a). Shielding off the UVB radiation range decreased the photochemical oxygen demand by 0–30%. Overall, however, no significant influence of UVB on the photochemical $O_2$ demand was detectable (Wilcoxon, $P = 0.4$, $n = 6$). Normalizing the photochemical $O_2$ demand to the DOC con-

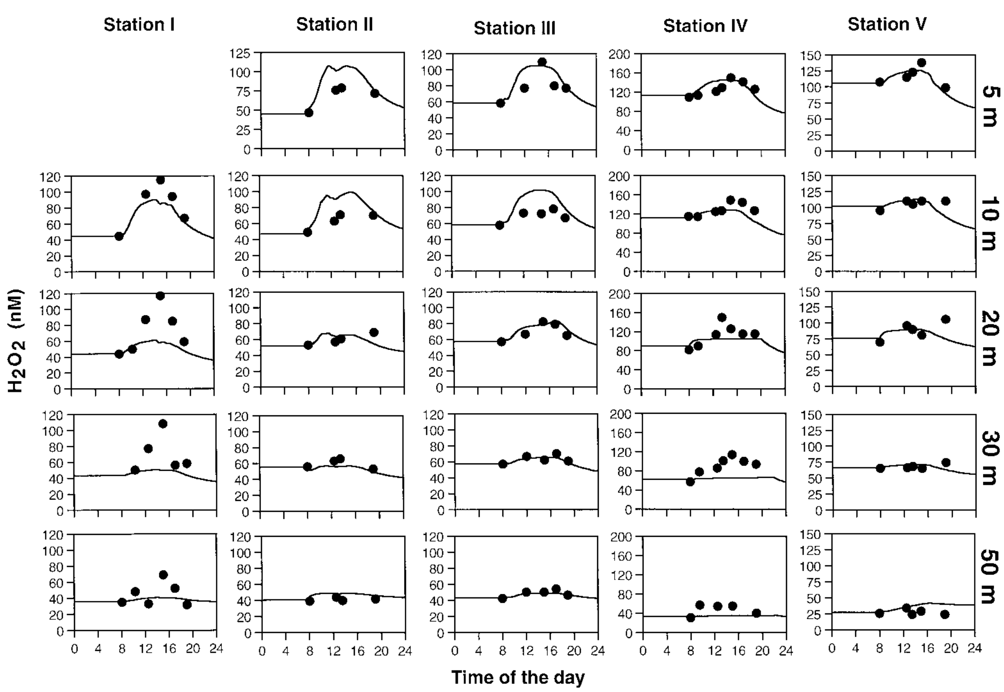


Fig. 2. Comparison of the observed (dots) and modeled (line) diurnal dynamics of $H_2O_2$ concentrations at different depth layers at Sta. I–V.

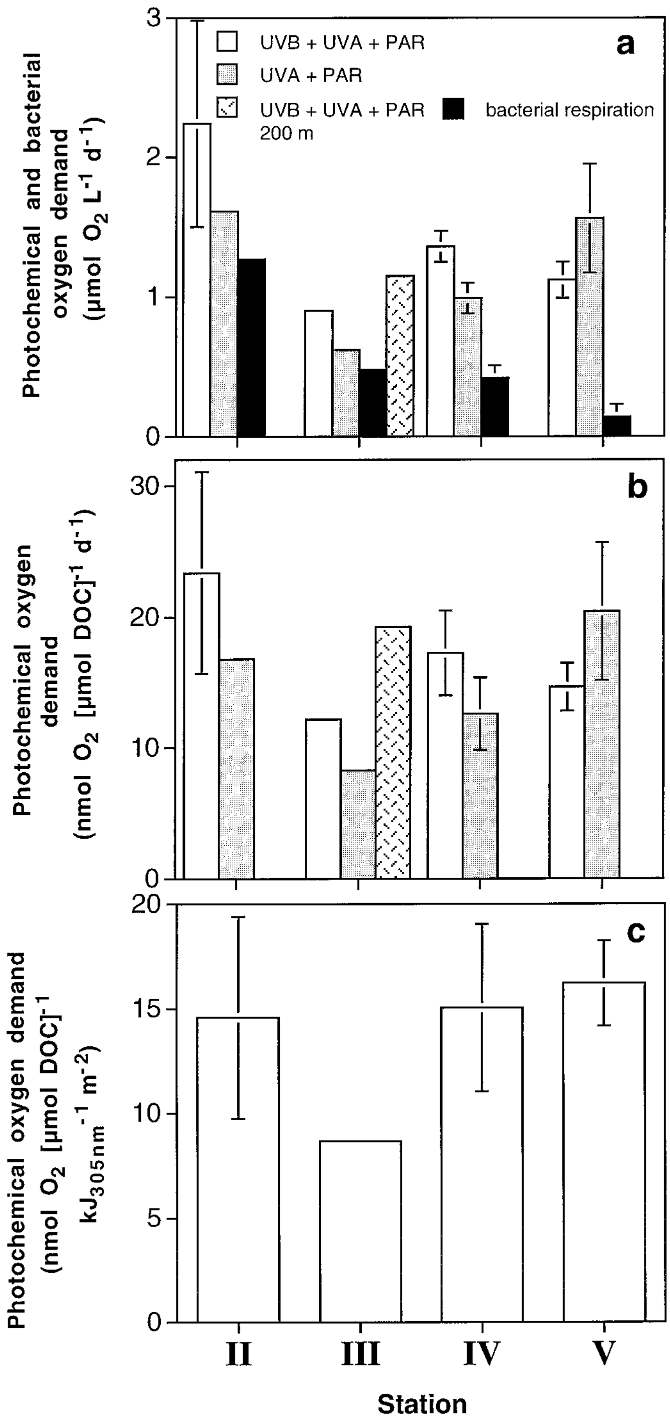


Fig. 3. Photochemical and bacterial oxygen demand (a)(in $\mu$mol $O_2$ $L^{-1}$ $d^{-1}$), as (b) DOC-normalized photochemical oxygen demand (in nmol $O_2$ $\mu$mol $DOC^{-1}$ $d^{-1}$), and (c) normalized to UVB radiation at the 305-nm wavelength. The water was sampled at the 10-m depth at Sta. II–V. At Sta. III, water was also sampled at the 200-m depth. For the photochemical oxygen demand, quartz BOD bottles were either exposed to full surface solar radiation or wrapped in Mylar-D foil to shield off the UVB range. Bacterial respiration was measured in the dark. Bars ($\pm$SD) represent means of two individual experiments performed on consecutive days. UVB = ultraviolet B; UVA = ultraviolet A; PAR = photosynthetic active radiation.

centration revealed that between 12 and 29 nmol $O_2$ $\mu$mol $DOC^{-1}$ $d^{-1}$ was consumed under surface solar radiation (Fig. 3b). The photochemical $O_2$ demand of water collected at 200 m in depth (at Sta. III, Fig. 3a) and exposed to the full range of surface solar radiation was about 20% higher when compared with water originating from a 10-m depth. This difference is more pronounced (~40% higher) if the $O_2$ demand is normalized to the DOC concentration (Fig. 3b). If the photochemical $O_2$ demand is normalized to the dose received at the 305-nm wavelength, only minor variations among Sta. II, IV, and V were detectable (Fig. 3c). Bacterial respiration consumed between 0.1 and 1.3 $\mu$mol $O_2$ $L^{-1}$ $d^{-1}$, amounting to 12–76% of the photochemical $O_2$ demand under the full range of surface solar radiation (Fig. 3a). Mean bacterial abundance in the upper–70-m water layer of Sta. II—V was about $5 \times 10^5$ cells $ml^{-1}$ (Kuipers et al. 2000).

## Discussion

Integrated daily surface irradiance of the specific UV wavelengths continuously decreased (by up to a twofold measure for the 305-nm wavelength) from the southernmost Sta. I toward the stations at higher latitudes. This latitudinal trend was not as pronounced for the integrated surface irradiance in the PAR range (Table 1). However, underwater irradiance was similar at Sta. I, IV, and V and was substantially higher (by an up to 2.7-fold measure) at Sta. II and III (as demonstrated for the 5-m depth layer in Table 1). Only $Kd_{305\ nm}$ was found to be significantly lower at Sta. III compared to the other stations (Table 2). Similarly, DOM fluorescence of the upper–50-m water layer was lowest at Sta. II and III (Table 4).

The diurnal stratification was detectable at all stations for the uppermost 10–50-m depth layer (Fig. 1). Although models have been established to describe the development of diurnal thermoclines (Imberger 1985; Price et al. 1986), there are only a few reports on in situ measurements. Price et al. (1986) describe the development of a diurnal thermocline in the Pacific Ocean reaching to a 40-m depth, whereas in freshwater systems, diurnal stratification extends only down to ~5 m in depth (Imberger 1985; Scully and Vincent 1997). At Sta. I, IV, and V, diurnal thermoclines were relatively shallow (~10 m in depth), whereas they reached 20 and 50 m in depth at Sta. II and III, respectively (Fig. 1).

*Diurnal dynamics of $H_2O_2$*—A distinct diurnal pattern was found at all stations, with highest $H_2O_2$ concentrations during mid- to late afternoon and lowest concentrations in the morning. The diurnal range in $H_2O_2$ concentration in the top surface layer was, on average, 42 nM, a value that corresponds to previously reported values ranging from 25 to 40 nM at different oceanic sites (Zika et al. 1985; Palenik and Morel 1988; Miller and Kester 1994). In situ $H_2O_2$ net production rates varied between 1 and 5.5 nmol $L^{-1}$ $h^{-1}$ (for the 40- and 5-m layers, respectively) (Table 5) and are comparable to those reported by Miller and Kester (1994) from the Saragasso Sea (~4 nM at 1- and 3-m depths). For comparison, the modeled $H_2O_2$ production rates are given in Table 5 as well. Integrating the in situ $H_2O_2$ net production rates obtained from the measured increase in $H_2O_2$ concentrations at the individual depth layers down to a 50-m depth over the diurnal cycle, a $H_2O_2$ net production of 38 $\mu$mol m$^{-2}$ d$^{-1}$ for Sta. II and III is obtained (Table 5). Integrated $H_2O_2$ net production calculated from the modeled net production rates varies between 26 and 58 $\mu$m m$^{-2}$ d$^{-1}$ for the five stations (Table 5).

In situ $H_2O_2$ net production rates at the 5-m depth, calculated from the increase in $H_2O_2$ concentration over the daytime period, were almost 10 times lower compared to the $H_2O_2$ production rates in 0.2-$\mu$m–filtered seawater exposed to surface solar radiation. This difference can be explained by the rapid attenuation, particularly that of the UVB wavelength range (Table 1). In addition, in situ decomposition of $H_2O_2$ and physical transport may contribute to the observed difference between the in situ net production and in the 0.2-$\mu$m–filtered seawater. The latter resembles gross $H_2O_2$ production, since the photodecomposition of $H_2O_2$ amounts to only ~5% of the $H_2O_2$ photoproduction rate (Moffett and Zafiriou 1993). However, net production rates calculated from the increase in $H_2O_2$ in the top–50-cm water layer at Sta. IV and V between 1230 and 1500 h resulted in in situ $H_2O_2$ production rates of 42 and 30 nmol L$^{-1}$ h$^{-1}$, respectively, and were thus similar to the $H_2O_2$ gross production rates (39.8 ± 12.5 nmol L$^{-1}$ h$^{-1}$). The depth limit of diurnal variations in $H_2O_2$ concentration was variable, ranging between the 10% surface solar radiation level of the 340- and 380-nm wavelengths, corresponding to a depth of ~30–60 m. Scully and Vincent (1997) defined the depth limit of $H_2O_2$ production in a subarctic lake at the 1% depth of the 380-nm wavelength, which would correspond to a depth of 112–150 m at the stations sampled in the subtropical Atlantic. At these depth layers, however, we did not observe diurnal patterns in $H_2O_2$.

In order to determine whether the decrease in $H_2O_2$ concentration in surface waters in the late afternoon is caused by downward mixing or by biologically mediated decay, we can compare the depth-integrated (0–100-m) $H_2O_2$ concentrations at different times of the day at Sta. III. The depth-integrated $H_2O_2$ concentration was highest at 1500 h and did not exhibit a significant decrease until 1700 h. A 20% decrease in $H_2O_2$ concentration integrated over the 0–100-m depth was observed between 1700 and 1900 h. A subsurface maximum in $H_2O_2$ concentration was detectable at 1500 h, and this was followed by a rapid decrease until 1700 h in the upper–50-m water layer (Fig. 1). The constant depth-integrated $H_2O_2$ concentration between 1500 and 1700 h indicates that, at least over this time period, mixing events might account for the rapid decline in $H_2O_2$ in the top–10-m water layer.

This is consistent with the result obtained from our model. In order to define the relative contribution of biological versus physical processes for the modeled $H_2O_2$ concentrations, which were similar to in situ $H_2O_2$ concentrations at different depth layers during the course of the day (*see Fig. 2, Table 5*), we calculated the $H_2O_2$ loss ratio ($R_L$) as follows

$$R_L = \frac{L_{BD}}{L_{BD} + L_T}$$

where $L_{BD}$ is the loss of $H_2O_2$ due to biological degradation

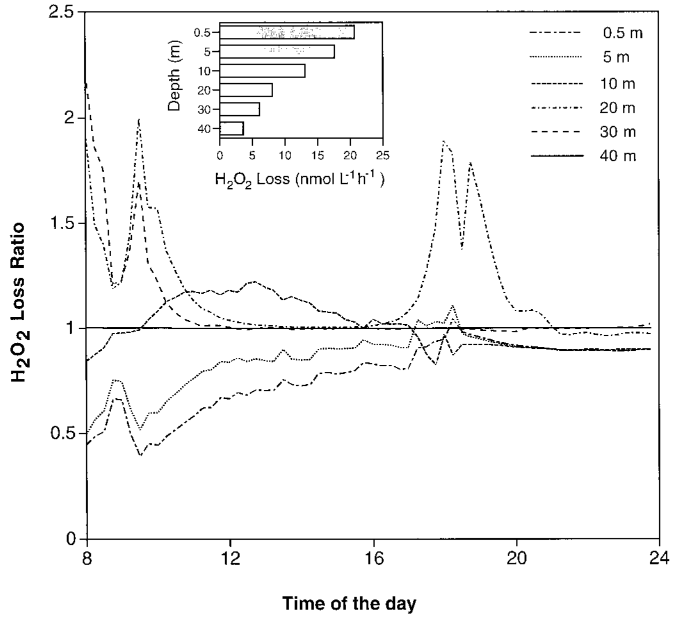


Fig. 4. Diurnal changes of the $H_2O_2$ loss ratio ($R_L$, *see Discussion for details*). A $R_L$ of 0.5 indicates that biological degradation and physical transport are equally important, whereas at a $R_L$ of 1, transport is negligible. A $R_L$ of >1 indicates that transport processes are responsible for the import of $H_2O_2$ to the respective depth layer. The inset shows the loss of $H_2O_2$ derived from the model (in nmol L$^{-1}$ h$^{-1}$), averaged over the time period between 0800 and 2400 h, resulting from both biological degradation and transport processes.

and $L_T$ is the net downward transport of $H_2O_2$. The term $L_T$ is negative if import of $H_2O_2$ to the respective depth layer takes place. The transport of $H_2O_2$ can be mediated by vertical mixing and diffusion. A $R_L$ of 0.5 indicates that both processes (biological degradation and physical transport) are of similar importance, whereas at a $R_L$ of 1, the net effect of transport on the $H_2O_2$ concentration is negligible (Fig. 4). A $R_L$ of >1 indicates that transport processes are responsible for the import of $H_2O_2$ to the respective depth layer. As indicated in Fig. 4, the significance of physical transport in exporting $H_2O_2$ is restricted to the upper–5-m water layer during the day. In this depth layer, physical transport and biological degradation are of similar importance in the morning, and the contribution of biological degradation increases in the afternoon (as indicated by ratios of >0.5). In the 10–30-m depth layer, a $R_L$ of >1 indicates the import of $H_2O_2$ as a result of transport processes. A pronounced diurnal pattern becomes obvious in the 20- and 30-m depth layer, where $R_L$ are ~1 between 1200 and 1600 h. The $R_L$ is >1 in both layers in the morning and in the 20-m depth layer in the late afternoon. Concomitantly, in the upper–5-m depth layer, the $R_L$ is <1 (Fig. 4). This indicates that in the morning and in the late afternoon, transport processes are primarily responsible for the export of $H_2O_2$ from the 5-m depth layer and for the import of $H_2O_2$ to the 20–30-m depth layer, whereas around noon these transport processes are negligible. This is consistent with the observed establishment of a diurnal thermocline that entraps DOM photoproducts in these layers for several hours during the period of high solar radiation. According to the model, the $R_L$ is ~1 at a 30-m depth from

1200 h onwards and at a 40-m depth during the entire course of the day, indicating that the diurnal photochemical production of $H_2O_2$ is matched by biological degradation (Fig. 4). In order to illustrate the quantitative importance of biological degradation of $H_2O_2$ versus transport processes at distinct depth layers, the modeled absolute loss of $H_2O_2$ resulting from both processes is shown in the inset in Fig. 4. Similar to $H_2O_2$ photoproduction, the $H_2O_2$ loss rates resulting from biological degradation and transport processes decrease with depth.

*Photochemical $O_2$ demand*—Photochemical $O_2$ demand of surface water DOM at the five stations varied between 0.9 and 2.8 $\mu$mol $O_2$ $L^{-1}$ $d^{-1}$, or between 0.1 and 0.3 $\mu$mol $O_2$ $L^{-1}$ $h^{-1}$, assuming a 12-h photoperiod. Similar values are reported by Laane et al. (1985) from an oligotrophic station in the coastal Caribbean Sea. Most studies on photochemical $O_2$ demand, however, were conducted in humic-rich freshwater systems (Lindell and Rai 1994; Amon and Benner 1996; Reitner et al. 1997), yielding up to ~40-fold higher photochemical $O_2$ consumption rates compared with those obtained during our study. However, DOC-normalized photochemical $O_2$ demand between the open Atlantic Ocean and the humic-rich freshwater systems differs only by a factor of about two to five, indicating substantial concentrations of photoreactive DOM in the surface waters of the subtropical Atlantic. DOC-normalized photochemical $O_2$ demand of water collected at a 200-m depth was about 1.4-fold higher compared to that of water from the 10-m depth, which indicates that there is a higher contribution of photochemically reactive DOM to the bulk DOM pool in waters below the euphotic zone (Kieber et al. 1989; Mopper et al. 1991). This was also obvious from the significantly higher DOM fluorescence at the 150-m depth compared with that obtained at the 50-m depth (Table 4). Assuming that the photochemical $O_2$ demand roughly equals the decrease in DOC concentration (Amon and Benner 1996), ~1–3 $\mu$mol DOC $L^{-1}$ $d^{-1}$ are photochemically transformed to DIC in surface waters. This accounts for ~1–4% of the total DOC (assuming a mean surface water DOC concentration of ~80 $\mu$M, Table 4). A similar percentage has been found for the northern Adriatic Sea (1.6–5.0 $\mu$mol $O_2$ $L^{-1}$ $d^{-1}$; ~100 $\mu$M DOC)(Obernosterer and Herndl 2000). It has been demonstrated that the photochemical $O_2$ demand is directly correlated with the DOC concentration (Lindell and Rai 1994; Amon and Benner 1996). In our study, DOC concentrations in surface waters were similar (~80 $\mu$M) at all stations (Table 5) and therefore cannot explain the difference in photochemical $O_2$ demand. Relating the photochemical $O_2$ demand to the UVB dose received results in similar values for Sta. II, IV, and V, whereas at Sta. III, the DOC-normalized photochemical $O_2$ demand is lower. At Sta. III, both $Kd_{305\ nm}$ and DOM fluorescence have been found to be significantly lower compared to similar values for the other stations, indicating differences in the optical properties of the DOM at this station compared with the other stations.

Shielding off UVB radiation decreased the photochemical $O_2$ demand by 0–30% at Sta. II—IV; however, the overall contribution of UVB to the photochemical $O_2$ demand was not significant. The effect of UVB on the photochemical $O_2$ demand was most pronounced at Sta. II and III, where the intensity of surface UVB radiation was higher, as indicated by higher surface 305-nm : 340-nm wavelength ratios at Sta. II and III (~0.12) compared to similar values for Sta. IV and V (~0.08). Previous studies have shown that the UVB, UVA, and PAR ranges are roughly equally in terms of their contribution to the photooxidation (measured as photochemical production of inorganic carbon and photochemical $O_2$ demand) of humic-rich DOM (Graneli et al. 1996; Reitner et al. 1997). Surface water bacterial respiration was lower than the photochemical $O_2$ demand at all stations, amounting to about 12–76% of the photochemical $O_2$ demand. In contrast to that, in the northern Adriatic Sea, bacterial $O_2$ demand was about equal to the photochemical $O_2$ demand of surface waters, and in the coastal North Sea, bacterial $O_2$ demand was, on average, about threefold higher compared to the rates of photochemical $O_2$ demand of surface waters (Obernosterer and Herndl 2000).

Our results demonstrate that $H_2O_2$ is a sensitive tracer for photochemically driven processes, as indicated by the similar diurnal dynamics of $H_2O_2$ and DOM fluorescence. As indicated in this study, the development of a diurnal thermocline is important in structuring the uppermost water column, ultimately leading to the exposure of DOM to high irradiation intensities over almost an entire daylight period. Similar diurnal dynamics (as shown here for $H_2O_2$) can also be assumed for other photoproducts, and a number of these photoproducts are potentially available to bacterioplankton. Bacterioplankton activity has been shown to recover quickly from UV stress (Kaiser and Herndl 1997; Arrieta et al. 2000). If we assume that the response of the bacterioplankton activity to newly formed photoproducts is as fast as indicated in our model, the diurnally stratified water layer can be considered to be highly dynamic with respect to photochemical and biological processes.

## References

AMADOR, J. A., M. ALEXANDER, AND R. G. ZIKA. 1989. Sequential photochemical and microbial degradation of organic molecules bound to humic acids. Appl. Environ. Microbiol. **55:** 2843–2849.

AMON, R. M. W., AND R. BENNER. 1996. Photochemical and microbial consumption of dissolved organic carbon and dissolved oxygen in the Amazon River system. Geochim. Cosmochim. Acta **60:** 1783–1792.

ARRIETA, J. M., M. G. WEINBAUER, AND G. J. HERNDL. 2000. Interspecific variability in the sensitivity to ultraviolet radiation and subsequent recovery in selected isolates of marine bacteria. Appl. Environ. Microbiol. **66:** 1468–1473.

BENNER, R., AND B. BIDDANDA. 1998. Photochemical transformations of surface and deep marine dissolved organic matter: Effects on bacterial growth. Limnol. Oceanogr. **43:** 1373–1378.

———, AND M. STROM. 1993. A critical evaluation of the analytical blank associated with DOC measurements by high-temperature catalytic oxidation. Mar. Chem. **41:** 153–160.

BERTILSSON, S., AND L. J. TRANVIK. 1998. Photochemically produced carboxylic acids as substrates for freshwater bacterioplankton. Limnol. Oceanogr. **43:** 885–895.

BLUMBERG, A. F., AND G. L. MELLOR. 1987. A description of a three-dimensional coastal ocean circulation model, p. 1–16. *In*

N. S. Heaps [ed.], Three dimensional coastal ocean models. AGU.

BUSHAW, K. L., AND OTHERS. 1996. Photochemical release of biologically available nitrogen from aquatic dissolved organic matter. Nature **381:** 404–407.

COOPER, W. J., AND D. R. S. LEAN. 1989. Hydrogen peroxide concentration in a northern lake: Photochemical formation and diel variability. Environ. Sci. Technol. **23:** 1425–1428.

———, AND ———. 1992. Hydrogen peroxide in marine and fresh water systems, p. 527–535. *In* W. A. Nierenberg [ed.], Encyclopedia of Earth system science. Academic.

———, C. SHAO, D. R. S. LEAN, A. S. GORDON, AND J. F. E. SCULLY. 1994. Factors affecting the distribution of $H_2O_2$ in surface waters, p. 393–422. *In* L. A. Baker [ed.], Advances in chemistry series. American Chemical Society.

———, AND R. G. ZIKA. 1983. Photochemical formation of hydrogen peroxide in surface and ground waters exposed to sunlight. Science **220:** 711–712.

CRUTZEN, P. J. 1992. Ultraviolet on the increase. Nature **356:** 104–105.

CULLEN, J. C., P. J. NEALE, AND M. P. LESSER. 1992. Biological weighting function for the inhibition of phytoplankton photosynthesis by ultraviolet radiation. Science **258:** 646–650.

FRANCKO, D. A., AND R. T. HEATH. 1982. UV-sensitive complex phosphorus: Association with dissolved humic material and iron in a bog lake. Limnol. Oceanogr. **27:** 564–569.

GRANELI, W., M. LINDELL, AND L. TRANVIK. 1996. Photo-oxidative production of dissolved inorganic carbon in lakes of different humic content. Limnol. Oceanogr. **41:** 698–706.

HERNDL, G. J., G. MÜLLER-NIKLAS, AND J. FRICK. 1993. Major role of UV-B in controlling bacterioplankton growth in the surface layer of the ocean. Nature **361:** 717–719.

HOLM-HANSEN, O., D. LUBIN, AND E. W. HELBLING. 1993. Ultraviolet radiation and its effects on organisms in aquatic environments, p. 379–425. *In* A. R. Young [ed.], Environmental UV photobiology. Plenum.

IMBERGER, J. 1985. The diurnal mixed layer. Limnol. Oceanogr. **30:** 737–770.

KAISER, E., AND G. J. HERNDL. 1997. Rapid recovery of marine bacterioplankton activity after inhibition by UV radiation in coastal waters. Appl. Environ. Microbiol. **63:** 4026–4031.

KIEBER, D. J., J. M. DANIEL, AND K. MOPPER. 1989. Photochemical source of biological substrates in sea water: Implications for carbon cycling. Nature **341:** 637–639.

KIRK, J. T. O. 1994. Optics and UV-B radiation in natural waters. Arch. Hydrobiol. Beih. **43:** 1–16.

KUIPERS, B., G. J. VAN NOORT, J. VOSJAN, AND G. J. HERNDL. 2000. Diel periodicity of bacterioplankton in the euphotic zone of the subtropical Atlantic Ocean. Mar. Ecol. Prog. Ser. **201:** 13–25.

LAANE, R. W. P. M., W. W. C. GIESKES, G. W. KRAAY, AND A. EVERSDIJK. 1985. Oxygen consumption from natural waters by photo-oxidizing processes. Neth. J. Sea Res. **19:** 125–128.

LINDELL, M. J., AND H. RAI. 1994. Photochemical oxygen consumption in humic waters. Arch. Hydrobiol. Beih. **43:** 145–155.

MILLER, W. L., AND D. R. KESTER. 1988. Hydrogen peroxide measurement in seawater by (*p*-hydroxyphenyl)acetic acid dimerization. Anal. Chem. **60:** 2711–2715.

———, AND ———. 1994. Peroxide variations in the Saragasso Sea. Mar. Chem. **48:** 17–29.

———, AND R. G. ZEPP. 1995. Photochemical production of dissolved inorganic carbon from terrestrial organic matter: Significance to the oceanic organic carbon cycle. Geophys. Res. Lett. **22:** 417–420.

MOFFET, J. W., AND O. C. ZAFIRIOU. 1990. An investigation of hydrogen peroxide chemistry in surface waters of Vineyard Sound with $H_2{}^{18}O_2$ and ${}^{18}O_2$. Limnol. Oceanogr. **35:** 1221–1229.

———, AND ———. 1993. The photochemical decomposition of hydrogen peroxide in surface waters of the eastern Caribbean and Orinoco River. J. Geophys. Res. **98:** 2307–2313.

———, AND R. G. ZIKA. 1983. Oxidation kinetics of Cu(I) in seawater: Implications for its existence in the marine environment. Mar. Chem. **13:** 239–251.

MOPPER, K., X. ZHOU, R. J. KIEBER, D. J. KIEBER, R. J. SIKORSKI, AND R. D. JONES. 1991. Photochemical degradation of dissolved organic carbon and its impact on the oceanic carbon cycle. Nature **353:** 60–62.

MORAN, M. A., AND R. G. ZEPP. 1997. Role of photoreactions in the formation of biologically labile compounds from dissolved organic matter. Limnol. Oceanogr. **42:** 1307–1316.

MORRIS, D. P., AND B. H. HARGREAVES. 1997. The role of photochemical degradation of dissolved organic carbon in regulating the UV transparency of three lakes on the Pocono Plateau. Limnol. Oceanogr. **42:** 239–249.

OBERNOSTERER, I., AND G. J. HERNDL. 2000. Differences in the optical and biological reactivity of the humic and nonhumic dissolved organic carbon component of two contrasting coastal marine environments. Limnol. Oceanogr. **45:** 1120–1129.

———, B. REITNER, AND G. J. HERNDL. 1999. Contrasting effects of solar radiation on dissolved organic matter and its bioavailability to marine bacterioplankton. Limnol. Oceanogr. **44:** 1645–1654.

PAI, S.-C., G.-C. GONG, AND K.-K. LIU. 1993. Determination of dissolved oxygen in seawater by direct spectrophotometry of total iodine. Mar. Chem. **41:** 343–351.

PALENIK, B., AND F. M. M. MOREL. 1988. Dark production of $H_2O_2$ in the Sargasso Sea. Limnol. Oceanogr. **33:** 1606–1611.

PALENIK, B., O. C. ZAFIRIOU, AND F. M. M. MOREL. 1987. Hydrogen peroxide production by a marine phytoplankter. Limnol. Oceanogr. **32:** 1365–1369.

PARSONS, T., Y. MAITA, AND C. LALLI. 1984. A manual of chemical and biological methods for seawater analysis. Pergamon.

PRICE, J. F., R. A. WELLER, AND R. PINKEL. 1986. Diurnal cycling: Observations and models of the upper ocean response to diurnal heating, cooling, and wind mixing. J. Geophys. Res. **91:** 8411–8427.

REITNER, B., G. J. HERNDL, AND A. HERZIG. 1997. Role of ultraviolet-B radiation on photochemical and microbial oxygen consumption in a humic-rich shallow lake. Limnol. Oceanogr. **42:** 950–960.

ROLAND, F., N. F. CARACO, J. J. COLE, AND P. DELGIORGIO. 1999. Rapid and precise determination of dissolved oxygen by spectrophotometry: Evaluation of interference from color and turbidity. Limnol. Oceanogr. **44:** 1148–1154.

RONCEL, M., J. A. NAVARRO, AND M. D. L. ROSA. 1989. Coupling of solar energy to hydrogen peroxide production in the Cyanobacterium *Anacystis nidulans.* Appl. Environ. Microbiol. **55:** 483–487.

SCULLY, N. M., AND W. F. VINCENT. 1997. Hydrogen peroxide: A natural tracer of stratification and mixing processes in subarctic lakes. Arch. Hydrobiol. **139:** 1–15.

SIKORSKI, R. J., AND R. G. ZIKA. 1993. Modeling mixed-layer photochemistry of $H_2O_2$: Optical and chemical modeling of production. J. Geophys. Res. **98:** 2315–2328.

SMITH, R. C. 1989. Ozone, middle ultraviolet radiation and the aquatic environment. Photochem. Photobiol. **50:** 459–468.

STOLARSKI, R., R. BOJKOV, L. BISHOP, C. ZEREFOS, J. STAEHELIN, AND J. ZAWODNY. 1992. Measured trends in stratospheric ozone. Science **256:** 342–349.

TRANVIK, L., AND S. KOKALJ. 1998. Decreased biodegradability of algal DOC due to interactive effects of UV radiation and humic matter. Aquat. Microb. Ecol. **14:** 301–307.

VODACEK, A. 1992. An explanation of the spectral variation in freshwater CDOM fluorescence. Limnol. Oceanogr. **37:** 1808–1813.

WELLER, R., AND O. SCHREMS. 1993. $H_2O_2$ in the marine troposphere and seawater of the Atlantic Ocean. Geophys. Res. Lett. **20:** 125–128.

WILKINSON, L. 1990. SYSTAT: The system for statistics. SYSTAT, Inc.

ZAFIRIOU, O. C., J. JOUSSOT-DUBIEN, R. G. ZEPP, AND R. G. ZIKA. 1984. Photochemistry of natural waters. Environ. Sci. Technol. **18:** 358A–371A.

ZIKA, R. G., J. W. MOFFET, R. G. PETASNE, W. J. COOPER, AND E. S. SALTZMAN. 1985. Spatial and temporal variations of hydrogen peroxide in Gulf of Mexico waters. Geochim. Cosmochim. Acta **49:** 1173–1184.

*Received: 23 February 2000*
*Accepted: 24 October 2000*
*Amended: 7 November 2000*